# The nuclear-spin-forbidden rovibrational transitions of water from first principles



Cite as: J. Chem. Phys. (in press) (2022); https://doi.org/10.1063/5.0090771
Submitted: 09 March 2022 • Accepted: 04 May 2022 • Accepted Manuscript Online: 04 May 2022

Andrey Yachmenev, Guang Yang, Emil Zak, et al.



Accepted to J. Chem. Phys. 10.1063/5.0090771

# The nuclear-spin-forbidden rovibrational transitions of water from first principles

Andrey Yachmenev,[1,2,a)] Guang Yang,[1,3] Emil Zak,[1] Sergei Yurchenko,[4] and Jochen Küpper[1,2,3]
[1)] *Center for Free-Electron Laser Science CFEL, Deutsches Elektronen-Synchrotron DESY, Notkestr. 85, 22607 Hamburg, Germany*
[2)] *Center for Ultrafast Imaging, Universität Hamburg, Luruper Chaussee 149, 22761 Hamburg, Germany*
[3)] *Department of Physics, Universität Hamburg, Luruper Chaussee 149, 22761 Hamburg, Germany*
[4)] *Department of Physics and Astronomy, University College London, Gower Street, WC1E 6BT London, United Kingdom*

(Dated: 2022-05-02)

The water molecule occurs in two nuclear-spin isomers that differ by the value of the total nuclear spin of the hydrogen atoms, i. e., $I = 0$ for *para*-$H_2O$ and $I = 1$ for *ortho*-$H_2O$. Spectroscopic transitions between rovibrational states of *ortho* and *para* water are extremely weak due to the tiny hyperfine nuclear-spin-rotation interaction of only ∼30 kHz and so far were not observed. We report the first comprehensive theoretical investigation of the hyperfine effects and *ortho-para* transitions in $H_2{}^{16}O$ due to nuclear-spin-rotation and spin-spin interactions. We also present the details of our newly developed general variational approach to the simulation of hyperfine effects in polyatomic molecules. Our results for water suggest that the strongest *ortho-para* transitions with room-temperature intensities on the order of $10^{-31}$ cm/molecule are about an order of magnitude larger than previously predicted values and should be detectable in the mid-infrared $\nu_2$ and near-infrared $2\nu_1 + \nu_2$ and $\nu_1 + \nu_2 + \nu_3$ bands by current spectroscopy experiments.

## I. INTRODUCTION

Water is the third most abundant molecule in the universe. It is also quite unique in that it possesses a wide range of anomalous properties, some of which may be a result of nuclear spin symmetry breaking. It has two nuclear spin isomers, *ortho*, with a total nuclear spin of hydrogen atoms $I = 1$, and *para*, with a total nuclear spin of hydrogens $I = 0$. In isolated-molecule conditions the *ortho* and *para* nuclear spin isomers show tremendously long-lasting stability to inter-conversion,[1,2] can be spatially separated,[3,4] and exhibit distinct physical and chemical properties.[5,6] Thus the nuclear spin isomers of water are frequently treated as distinct molecular species.

The concept of stable nuclear spin isomers is appealing to astrophysicists, as it allows to deduce temperatures, below 50 K, in cometary comae, star- and planet-forming regions from the observations of relative abundance of *ortho* and *para* species.[7–11] Some astronomical observations however reported anomalous *ortho-para* ratios (OPR), corresponding to spin temperatures that are much lower than gas kinetic temperatures in the same region.[12–15] These observations pose the intriguing question if the OPR values could be altered as a result of internal *ortho-para* conversion, which can possibly be enhanced by natural factors, such as molecular collisions,[16–18] interaction with catalytic surfaces,[19] external fields[20] and radiation.[21] Low nuclear-spin temperatures have been attributed to the photodesorption of water from colder icy grains.[22] However, this theory was benchmarked and disputed in a number of recent laboratory experiments.[23–26] Arguably there could be another yet unknown mechanism of spin-non-destructive desorption of water molecules from ice.

The OPR values can change as a result of the interaction between the nuclear spins and an induced internal magnetic field of the rotating molecule, which is called the nuclear spin-rotation interaction. For the main water isotopologue $H_2{}^{16}O$, considered here, the $^{16}O$ has zero nuclear spin, and the hyperfine coupling between the spins of the protons is very weak, providing a fundamental rationale for neglecting the *ortho-para* conversion in practical applications. However, it can be significantly enhanced by accidental resonances between the *ortho* and *para* states, which are present in vibrationally excited bands of isolated water. Their coupling can be amplified by external effects such as molecular collisions and interactions with strong external fields and field gradients. The accurate modeling of these processes may unravel previously unknown mechanisms contributing to the observed anomalous OPR of water in space. Precise knowledge of the molecular hyperfine states and corresponding transitions is mandatory for the understanding of such conversion mechanisms. This information can also be important for cold-molecule precision spectroscopy relying on controlled hyperfine transitions and hyperfine-state changing collisions.[27]

Here, we report a complete linelist of rovibrational hyperfine transitions in $H_2{}^{16}O$ at room-temperature that we computed using an accurate variational approach[28–31] with an empirically refined potential energy surface (PES)[32] and a high-level *ab initio* spin-rotation tensor surface. The spin-spin coupling was modelled as the magnetic dipole-dipole interaction between the two hydrogen nuclei. We show that the strongest forbidden *ortho-para* transitions are on the order of $10^{-31}$ cm/molecule, which is about ten times stronger than previously reported calculations for the same lines.[2] We also present the details of

[a)] Email: andrey.yachmenev@cfel.de; URL: https://www.controlled-molecule-imaging.org

our variational approach for computing hyperfine effects, which is general and not restricted by the numbers and specific magnitudes of the molecules' nuclear spins.

## II. THEORETICAL DETAILS

### A. Spin-rotation and spin-spin coupling

In this section we describe the implementation of the nuclear spin-rotation and spin-spin coupling terms within the general variational framework of the nuclear motion approach TROVE.[28–31] Implementation details of the hyperfine nuclear quadrupole coupling can be found in our previous works.[33,34]

The spin-rotation coupling is the interaction between the rotational angular momentum $\mathbf{J}$ of the molecule and the nuclear spins $\mathbf{I}_n$ of different nuclei[35]

$$H_{\rm sr} = \sum_n^{N_I} \mathbf{I}_n \cdot \mathbf{M}_n \cdot \mathbf{J}, \tag{1}$$

where $\mathbf{M}_n$ is the second-rank spin-rotation tensor relative to the nucleus $n$ and the sum runs over all nuclei $N_I$ with non-zero spin. The interaction between the nuclear spins $\mathbf{I}_n$ of different nuclei is given by the spin-spin coupling as

$$H_{\rm ss} = \sum_{n>n'}^{N_I} \mathbf{I}_n \cdot \mathbf{D}_{n,n'} \cdot \mathbf{I}_{n'}, \tag{2}$$

where $\mathbf{D}_{n,n'}$ is the second-rank spin-spin tensor, which is traceless and symmetric. Using the spherical-tensor representation,[36] the spin-rotation and spin-spin Hamiltonians can be expressed as

$$H_{\rm sr} = \frac{1}{2}\sum_n^{N_I}\sum_{\omega=0}^{2} \sqrt{2\omega+1}\left(-\frac{1}{\sqrt{3}}\right)\mathbf{I}_n^{(1)} \cdot \left((-1)^\omega \left[\mathbf{M}_n^{(\omega)} \otimes \mathbf{J}^{(1)}\right]^{(1)} + \left[\mathbf{J}^{(1)} \otimes \mathbf{M}_n^{(\omega)}\right]^{(1)}\right) \tag{3}$$

and

$$H_{\rm ss} = \sum_{n>n'}^{N_I} \mathbf{D}_{n,n'}^{(2)} \cdot \left[\mathbf{I}_n^{(1)} \otimes \mathbf{I}_{n'}^{(1)}\right]^{(2)}, \tag{4}$$

where $\mathbf{M}_n^{(\omega)}$, $\mathbf{D}_{n,n'}^{(2)}$, $\mathbf{J}^{(1)}$, and $\mathbf{I}_n^{(1)}$ denote the spherical-tensor representations of operators in (1) and (2) and the square brackets are used to indicate the tensor product of two spherical-tensor operators. Because the spin-rotation tensor is generally not symmetric, the second term in the sum (3) is added to ensure that the Hamiltonian is Hermitian.

The nuclear-spin operator $\mathbf{I}_n$ and the rotational-angular-momentum operator $\mathbf{J}$ are coupled using a *nearly-equal* coupling scheme, i. e., $\mathbf{I}_{1,2} = \mathbf{I}_1 + \mathbf{I}_2$, $\mathbf{I}_{1,3} = \mathbf{I}_{1,2} + \mathbf{I}_3$, …, $\mathbf{I} \equiv \mathbf{I}_{1,N} = \mathbf{I}_{1,N-1} + \mathbf{I}_N$, and $\mathbf{F} = \mathbf{J} + \mathbf{I}$. The nuclear-spin functions $|I, m_I, \mathcal{I}\rangle$ depend on the quantum numbers $I$ and $m_I$ of the collective nuclear-spin operator $\mathbf{I}$ and its projection onto the laboratory $Z$ axis, respectively. The set of auxiliary quantum numbers $\mathcal{I} = \{I_1, I_{1,2}, I_{1,3}, \ldots, I_{1,N-1}\}$ for the intermediate spin angular momentum operators provide a unique assignment of each nuclear-spin state. The total spin-rovibrational wave functions $|F, m_F, u\rangle$ are built as symmetry-adapted linear combinations of the coupled products of the rovibrational wave functions $|J, m_J, l\rangle$ and the nuclear-spin functions $|I, m_I, \mathcal{I}\rangle$. Here, $J$ and $F$ are the quantum numbers of $\mathbf{J}$ and $\mathbf{F}$ operators with $m_J$ and $m_F$ of their $Z$-axis projections. $l$ and $u$ denote the rovibrational and hyperfine state indices, respectively, and embrace all quantum numbers, e. g., rotational $k$ and vibrational quantum numbers $v_1, v_2, \ldots$, that are necessary to characterize a nuclear spin-rovibrational state.

The symmetrization postulate requires the total wavefunction of the $H_2O$ molecule to change sign upon exchange of the protons, i. e., to transform as one of the irreducible representations $B_1, B_2$ of its $\mathbf{C}_{2v}$(M) symmetry group. Accordingly, the *ortho* spin state $|I = 1\rangle$ of $A_1$ symmetry can be coupled with the rovibrational states of $B_1$ and $B_2$ symmetries and the *para* state $|I = 0\rangle$ of $B_2$ symmetry can be coupled with the rovibrational states of $A_1$ and $A_2$ symmetries.

The matrix representations of the spin-rotation and spin-spin Hamiltonians in the basis of the $|F, m_F, u\rangle$ functions are diagonal in $F$ and $m_F$, with the explicit expressions given by

$$\begin{aligned}\langle F, m_F, u'|H_{\rm sr}|F, m_F, u\rangle &= \\ &= \frac{1}{2}(-1)^{I+F}\sqrt{(2J+1)(2J'+1)}\begin{Bmatrix} I' & J' & F \\ J & I & 1\end{Bmatrix} \\ &\times \sum_n^{N_I}\sum_{\omega=0}^{2} N_\omega \left[(-1)^\omega J \begin{Bmatrix} \omega & 1 & 1 \\ J & J' & J\end{Bmatrix}\begin{pmatrix} J & 1 & J \\ -J & 0 & J\end{pmatrix}^{-1}\right. \\ &\left. + J'\begin{Bmatrix} 1 & \omega & 1 \\ J & J' & J'\end{Bmatrix}\begin{pmatrix} J' & 1 & J' \\ -J' & 0 & J'\end{pmatrix}^{-1}\right] \\ &\times \mathcal{M}_{\omega,n}^{(J'l',Jl)}\langle I'||\mathbf{I}_n^{(1)}||I\rangle\end{aligned} \tag{5}$$

and

$$\begin{aligned}\langle F, m_F, u'|H_{\rm ss}|F, m_F, u\rangle &= \\ &= (-1)^{I+J'+J+F}\sqrt{(2J+1)(2J'+1)}\begin{Bmatrix} I' & J' & F \\ J & I & 2\end{Bmatrix} \\ &\times \sum_{n>n'}^{N_I} \mathcal{D}_{n,n'}^{(J'l',Jl)}\langle I'||[\mathbf{I}_n^{(1)} \otimes \mathbf{I}_{n'}^{(1)}]^{(2)}||I\rangle,\end{aligned} \tag{6}$$

with the normalization constant $N_\omega = 1$, $-\sqrt{3}$, and $\sqrt{5}$ for $\omega = 0$, 1, and 2, respectively. The expressions for the reduced matrix elements of the nuclear-spin operators $\langle I'||\mathbf{I}_n^{(1)}||I\rangle$ and $\langle I'||[\mathbf{I}_n^{(1)} \otimes \mathbf{I}_{n'}^{(1)}]^{(2)}||I\rangle$ depend on the total number of coupled spins and can be computed using a general recursive procedure as described, for example,

in ref. 33. Here, for the two equivalent hydrogen spins $I_1 = I_2 = 1/2$, the reduced matrix elements are

$$\langle I'||\mathbf{I}_n^{(1)}||I\rangle = (-1)^{I\delta_{n,1}+I'\delta_{n,2}} I_1 \times \sqrt{(2I+1)(2I'+1)} \begin{Bmatrix} I_1 & I' & I_1 \\ I & I_1 & 1 \end{Bmatrix} \begin{pmatrix} I_1 & 1 & I_1 \\ -I_1 & 0 & I_1 \end{pmatrix}^{-1}, \quad (7)$$

with the explicit values $\langle 0||\mathbf{I}_n^{(1)}||0\rangle = 0$, $\langle 1||\mathbf{I}_n^{(1)}||1\rangle = \sqrt{3/2}$, $\langle 0||\mathbf{I}_n^{(1)}||1\rangle = \pm\sqrt{3}/2$ for $n = 1$ and 2, respectively, and $\langle 1||\mathbf{I}_n^{(1)}||0\rangle = \mp\sqrt{3}/2$.

The expressions for the $\mathcal{M}_{\omega,n}^{(J'l',Jl)}$ and $\mathcal{D}_{n,n'}^{(J'l',Jl)}$ tensors in Eqs. (5) and (6) depend on the chosen rovibrational wave functions $|J, m_J, l\rangle$, which are represented by the molecular rovibrational eigenfunctions calculated with the variational approach TROVE. The functions $|J, m_J, l\rangle$ are linear combinations of products of vibrational wave functions $|\nu\rangle = |v_1, v_2, \ldots, v_M\rangle$ ($M$ is the number of vibrational modes) and symmetric-top rotational functions

$$|J, m_J, l\rangle = \sum_{\nu,k} c_{\nu,k}^{(J,l)} |\nu\rangle |J, k, m_J\rangle . \quad (8)$$

In this basis, the $\mathcal{M}_{\omega,n}^{(J'l',Jl)}$ and $\mathcal{D}_{n,n'}^{(J'l',Jl)}$ tensors are

$$\mathcal{M}_{\omega,n}^{(J'l',Jl)} = \sum_{\nu'k'}\sum_{\nu k} \left[c_{\nu'k'}^{(J',l')}\right]^* c_{\nu k}^{(J,l)} (-1)^{k'} \times \sum_{\sigma=-\omega}^{\omega} \sum_{\alpha,\beta=x,y,z} \begin{pmatrix} J & \omega & J' \\ k & \sigma & -k' \end{pmatrix} U_{\omega\sigma,\alpha\beta}^{(2)} \langle\nu'|\bar{M}_{\alpha\beta,n}|\nu\rangle \quad (9)$$

and

$$\mathcal{D}_{n,n'}^{(J'l',Jl)} = \sum_{\nu'k'}\sum_{\nu k} \left[c_{\nu'k'}^{(J',l')}\right]^* c_{\nu k}^{(J,l)} (-1)^{k'} \times \sum_{\sigma=-2}^{2} \sum_{\alpha,\beta=x,y,z} \begin{pmatrix} J & 2 & J' \\ k & \sigma & -k' \end{pmatrix} U_{2\sigma,\alpha\beta}^{(2)} \langle\nu'|\bar{D}_{\alpha\beta,nn'}|\nu\rangle \quad (10)$$

where $\bar{M}_{\alpha\beta,n}$ and $\bar{D}_{\alpha\beta,nn'}$ ($\alpha,\beta = x,y,z$) are spin-rotation and spin-spin interaction tensors in the molecule-fixed frame and the $9\times 9$ constant matrix $U_{\omega\sigma,\alpha\beta}^{(2)}$ ($\omega = 0,\ldots,2$, $\sigma = -\omega,\ldots,\omega$) defines the transformation of a general second-rank Cartesian tensor operator into its spherical-tensor representation, see, e. g., (5.41)–(5.44) in ref. 36.

The total Hamiltonian $H$ is composed of a sum of the pure rovibrational Hamiltonian $H_{\rm rv}$ and hyperfine terms $H_{\rm sr}$ and $H_{\rm ss}$. In the basis of TROVE wave functions, the rovibrational Hamiltonian $H_{\rm rv}$ is diagonal, its elements are given by the rovibrational energies

$$\begin{aligned}\langle F, m_F, u'|H|F, m_F, u\rangle &= E_u\delta_{u,u'} + \langle F, m_F, u'|H_{\rm sr}|F, m_F, u\rangle \\ &\quad + \langle F, m_F, u'|H_{\rm ss}|F, m_F, u\rangle, \end{aligned} \quad (11)$$

where $\delta_{u,u'} = \delta_{J,J'}\delta_{l,l'}\delta_{I,I'}\delta_{\mathcal{I},\mathcal{I}'}$.

The above equations were implemented in the `hyfor` module of the Python software package Richmol,[37,38] which uses rovibrational molecular states calculated in TROVE as a variational basis. Alternative approaches using Watson-type effective Hamiltonians[39] are also implemented in the Richmol package.

The hyperfine energies and wave functions are computed in a three step procedure. First, we solve the full rovibrational problem using TROVE and obtain the rovibrational energies and wave functions for all states with energies below a selected threshold. In the next step, the rovibrational matrix elements of the spin-rotation and spin-spin tensors are computed in the form given by Eqs. (9) and (10). These matrix elements are later used to build the spin-rotation and spin-spin interaction Hamiltonians using Eqs. (5) and (6). The total Hamiltonian is composed of the sum of a purely rovibrational part, which is diagonal and given by the rovibrational state energies, and non-diagonal spin-rotation and spin-spin parts. In the final step, the hyperfine energies and wave functions are obtained by diagonalizing the total Hamiltonian.

The computation of the dipole transition intensities also proceeds in two steps. First, the rovibrational matrix elements of the dipole moment surface are computed and cast into a tensor form similar to (10),

$$\mathcal{K}_{\omega}^{(J'l',Jl)} = \sum_{\nu'k'}\sum_{\nu k} \left[c_{\nu'k'}^{(J',l')}\right]^* c_{\nu k}^{(J,l)} (-1)^{k'} \times \sum_{\sigma=-\omega}^{\omega} \sum_{\alpha,\beta=x,y,z} \begin{pmatrix} J & \omega & J' \\ k & \sigma & -k' \end{pmatrix} U_{\omega\sigma,\alpha}^{(1)} \langle\nu'|\bar{\mu}_{\alpha}|\nu\rangle, \quad (12)$$

where $\bar{\mu}_\alpha$ ($\alpha = x,y,z$) is the permanent dipole moment in the molecule-fixed frame and the $3\times 3$ constant matrix $U_{\omega\sigma,\alpha}^{(1)}$ ($\omega = 1$, $\sigma = -\omega,\ldots,\omega$) defines the transformation of a general first-rank Cartesian tensor operator into its spherical-tensor representation, see, e. g., (5.4) in ref. 36. In the second step, the dipole matrix elements are transformed into the basis of hyperfine wave functions, i. e.,

$$\mathcal{K}_{\omega}^{(F',u',F,u)} = \sum_{I',\mathcal{I}',J',l'}\sum_{I,\mathcal{I},J,l} \left[c_{I',\mathcal{I}',J',l'}^{(F',u')}\right]^* c_{I,\mathcal{I},J,l}^{(F,u)} (-1)^{I} \times \sqrt{(2J'+1)(2J+1)} \begin{Bmatrix} J' & F' & I \\ F & J & \omega \end{Bmatrix} \mathcal{K}_{\omega}^{(J',l',J,l)} \delta_{I',I}\delta_{\mathcal{I}',\mathcal{I}}, \quad (13)$$

where $c_{I,\mathcal{I},J,l}^{(F,u)}$ are hyperfine wave function coefficients obtained by diagonalization of the total Hamiltonian. Finally, the line strengths for transitions between hyperfine states $|f\rangle = |F', u'\rangle$ and $|i\rangle = |F, u\rangle$ are computed as[34]

$$S(f \leftarrow i) = (2F'+1)(2F+1) \left|\mathcal{K}_1^{(F'u',Fu)}\right|^2, \quad (14)$$

where we sum over all degenerate $m_F$ and $m_F'$ components. The expression for the integrated absorption coefficient

of the dipole transition in units of cm/molecule reads

$$I(f \leftarrow i) = \frac{8\pi^3 \nu_{if} e^{-hcE_i/kT}\left(1 - e^{-hc\nu_{if}/kT}\right)}{3hcZ(T)} S(f \leftarrow i), \tag{15}$$

where $\nu_{if} = |E_i - E_f|$ is the transition wavenumber, $E_i$ and $E_f$ are energy term values of the initial and final states in $\mathrm{cm}^{-1}$, $Z(T)$ is the temperature dependent partition function, $h$ (erg·s) is the Planck constant, $c$ (cm/s) is the speed of light and $k$ (erg/K) is the Boltzmann constant.

### B. Electronic structure calculations

The molecule-fixed frame spin-rotation tensors $\bar{M}_{\alpha\beta,n}$ ($\alpha, \beta = x, y, z$, $n = 1, 2$) were calculated *ab initio* on a grid of 2000 different molecular geometries with electronic energies ranging up to 30 000 $\mathrm{cm}^{-1}$ above the equilibrium energy. We used the all-electron CCSD(T) (coupled-cluster singles, doubles, and perturbative triples) method with the augmented core-valence correlation-consistent basis set aug-cc-pwCVTZ[40] and aug-cc-pVTZ[41,42] for the oxygen and hydrogen atoms, respectively. The basis sets were downloaded from the Basis Set Exchange library.[43–45] The calculations employed second-order analytical derivatives[46] together with the rotational London orbitals,[47,48] as implemented in the quantum chemistry package CFOUR.[49]

The electronic structure calculations used the principal axes of inertia coordinate frame. For variational calculations another frame was employed, defined such that the $x$ axis is parallel to the bisector of the valence bond angle with the molecule lying in the $xz$ plane at all instantaneous molecular geometries. In this frame, the $z$ axis coincides with the molecular axis at the linear geometry. The computed spin-rotation tensors were rotated from the principal axis of inertia to the new frame. The permutation symmetry is such, that exchange of the two hydrogen atoms transforms $\bar{M}_{\alpha\beta,1}$ into $\bar{M}_{\alpha\beta,2}$ followed by a sign change for non-diagonal elements ($\alpha \neq \beta$).

The expression for the spin-rotation tensor, as computed in CFOUR, contains multiplication by the inverse of the tensor of inertia, see (3) and (7) in ref. 48. For linear and closely linear geometries of the molecule, the inertial tensor becomes singular, which creates a discontinuity in the dependence of $xz$ and $zz$ elements of spin-rotation tensor on the bending angle. To circumvent this problem, we have multiplied the computed spin-rotation tensors on the right side by the corresponding inertial tensors. The resulting data for the inertia-scaled spin-rotation tensor was parameterized through least-squares fitting, using a power series expansions to fourth order in terms of valence bond coordinates, with $\sigma_{\mathrm{rms}} \leq 0.3$ kHz for all tensor components. Later, when computing the rovibrational matrix elements of the spin-rotation tensor, we have multiplied the inertia-scaled tensor with the inverse moment of inertia. The divergence of the spin-rotation tensor in the vicinity of linear geometries is exactly canceled by the basis functions chosen to satisfy the kinetic cusp condition at the linear geometry.[31,50]

The spin-spin tensor elements were computed as magnetic dipole-dipole interaction between two hydrogen nuclei $\mathrm{H}_1$ and $\mathrm{H}_2$,

$$D_{\alpha\beta,12} = \frac{\mu_0}{4\pi} \frac{\mu_1 \mu_2}{I_1 I_2 r_{12}^3} \left(\mathbf{I} - 3\mathbf{n} \otimes \mathbf{n}\right)_{\alpha\beta}, \tag{16}$$

where $\mu_1 = \mu_2 = 2.79284734$ are the magnetic dipole moments of $\mathrm{H}_1$ and $\mathrm{H}_2$ in units of the nuclear magneton, $I_1 = I_2 = 1/2$ are the corresponding hydrogen nuclear spins, $r_{12}$ is the distance between the hydrogen nuclei, and $\mathbf{n}$ is the unit vector directed from one hydrogen to another. The indirect spin-spin coupling constants mediated by the electronic motions were not considered here, as they are typically two orders of magnitude smaller than the direct constants.[51]

The magnitudes of the equilibrium *ab initio* spin-rotation and direct spin-spin diagonal tensor elements are about 30 and 60 kHz, respectively.[52] However, the corresponding matrix elements have different selection rules. In particular, due to the traceless-tensor nature of the spin-spin interaction, it can couple only states with $|J - J'| = 2$, see (6) and (10). The spin-rotation interaction can in principle couple states with $|J - J'| \leq 2$, where the *ortho-para* interaction between states with $|J - J'| \leq 1$ and $|k - k'| = 1$ occurs due to antisymmetric behavior of the off-diagonal elements of the spin-rotation tensor with respect to the proton exchange, i. e., $\bar{M}_{xz,1} = \bar{M}_{zx,2}$, see (5) and (9).

### C. Nuclear motion calculations

We employed TROVE to calculate the rovibrational states using the exact kinetic-energy operator formalism recently developed for triatomic molecules.[50] This formalism is based on the use of associated Laguerre polynomials $L_n^l(x)$ as bending basis functions, which ensures a correct behavior of the rovibrational wave functions at linear molecular geometry.[50] The bisecting frame embedding was selected as a non-rigid reference frame, with the $x$ axis oriented parallel to the bisector of the valence bond angle and the molecule placed in the $xz$ plane. In this frame, the $z$ axis coincides with the linearity axis at linear molecular geometry. Accurate empirically refined PES of $\mathrm{H}_2^{16}\mathrm{O}$ was employed.[32]

The primitive-stretching vibrational basis functions were generated by numerically solving the corresponding one-dimensional Schrödinger equations on a grid of 2000 points using the Numerov-Cooley approach.[53,54] The primitive basis functions were then symmetry-adapted to the irreducible representations of the $\mathbf{C}_{2\mathrm{v}}(\mathrm{M})$ molecular symmetry group using an automated numerical procedure.[30] The total vibrational basis set was formed as a direct product of the symmetry-adapted stretching and bending basis functions, contracted to include

states up to a polyad 48. It was used to solve the $J = 0$ eigenvalue problem for the complete vibrational Hamiltonian of $H_2O$. A product of the $J = 0$ eigenfunctions and symmetry-adapted rigid rotor wavefunctions formed the final rovibrational basis set. The rovibrational wavefunctions $|J, m_J, l\rangle$ for rotational excitations up to $J = 40$ and four irreducible representations $A_1$, $A_2$, $B_1$ and $B_2$ were computed by diagonalizing the matrix representation of the total rovibrational Hamiltonian $H_{\rm rv}$ in the rovibrational basis set. More details about the variational approach and the basis-symmetrization procedure for the case of triatomic molecules can be found in ref. 50.

### D. Linelist simulations

The linelist of hyperfine rovibrational transitions for $H_2^{16}O$ was computed with an energy cutoff at 15 000 cm$^{-1}$ and includes transitions up to $F = 39$ ($J = 40$). To further improve the accuracy of the linelist, after solving the pure rovibrational problem and before entering the hyperfine calculations, the rovibrational energies $E_u$ in (11) were replaced with the high-resolution experimental IUPAC values from ref. 55, where available. Such empirical adjustment of the rovibrational energies have been adopted and tested, e. g., for the production of molecular linelists as part of the ExoMol project.[56] Recently, this approach was proven accurate for computing the ultra-weak quadrupole transitions in water[57,58] and carbon dioxide,[59,60] which enabled their first laboratory ($H_2O$ and $CO_2$) and astrophysical ($CO_2$) detection.

The final linelist has been calculated at room temperature ($T = 296$ K) with the corresponding partition function $Z = 174.5813$,[61] and a threshold of $10^{-36}$ cm/molecule for the absorption intensity based on (15). The linelist stored in the ExoMol[62] format is provided in the supplementary information.

## III. RESULTS AND DISCUSSION

An overview of the calculated $H_2^{16}O$ dipole absorption stick spectrum at $T = 296$ K is shown in Fig. 1. The forbidden *ortho-para* transitions are plotted as red circles. Despite being, at least, 10 orders of magnitude weaker than the corresponding allowed transitions, for some of the strongest *ortho-para* transitions the predicted absorption intensities are close to the sensitivity threshold of modern cavity ring-down spectroscopic techniques.[64–66] All predicted *ortho-para* transitions with line intensity larger than $10^{-31}$ cm/molecule are listed in Table I. These transitions all occur in the fundamental $\nu_2$ bending and the overtone $2\nu_1 + \nu_2$ and $\nu_1 + \nu_2 + \nu_3$ bands. The off-diagonal elements of molecular-frame spin-rotation tensor $\bar{M}_{\alpha\beta,n}$, which lead to *ortho-para* interaction, are highly dependent on the bending vibrational coordinate, indicating significance of the $\nu_2$ band in *ortho-para* transitions. The size of the off-diagonal spin-rotation matrix elements

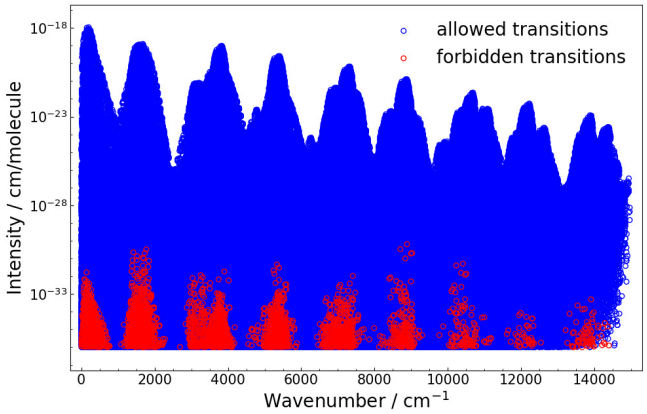


FIG. 1. Overview of the $H_2^{16}O$ dipole absorption spectrum at $T = 296$ K. The *ortho-ortho* and *para-para* transitions are marked with blue circles, whereas the *ortho-para* transitions are given by red circles.

increases for bending angles close to 180 °, i. e., the linear geometry of the molecule. This leads to an increase in the *ortho-para* interaction for rovibrational energies close to the linearity barrier at ∼8254 cm$^{-1}$ above the zero-point energy. The spin-rotation coupling in these vibrationally excited states is responsible for the *ortho-para* transitions. For example, the final transition state $F = 3$, $J_{k_a,k_c} = 4_{2,3}$ (ortho) with energy $E = 1908.016319$ cm$^{-1}$ is mixed with the state $F = 3$, $J_{k_a,k_c} = 3_{3,1}$ (para) with energy $E = 1907.450231$ cm$^{-1}$. The size of the rovibrational matrix element of spin-rotation tensor, $\mathcal{M}_{\omega,n}^{(J'l',Jl)}$ in (9) for this transitions is ±0.95 kHz and ±6.3 kHz (± for $n = 1, 2$) for $\omega = 1$ and 2, respectively. Note that following (5) only the spin-rotation tensor with $\omega = 1$ contributes to the *ortho-para* coupling. Allowed transitions into these states from the ground state are quite strong, $2.07 \times 10^{-20}$ and $3.52 \times 10^{-20}$ cm/molecule, respectively. Accordingly, intensity borrowing as a result of the spin-rotation interaction of excited states leads to non-zero intensities of the two corresponding forbidden transitions on the order of $10^{-31}$ molecule/cm. Similarly for other of the strongest forbidden transitions listed in Table I, the enhancement occurs due to intensity borrowing effect from strongly allowed transitions with coincident near resonance between the excited states, accompanied by a relatively large value of the spin-rotation matrix element $\mathcal{M}_{\omega=1,n}^{(J'l',Jl)}$.

Though *ortho-para* transitions are yet to be observed in $H_2O$, there are several spectroscopic studies of the allowed hyperfine transitions in the pure rotational spectrum of $H_2^{16}O$.[52,63,67,68] We used these data to validate the accuracy of our predictions. In Fig. 2 the calculated transitions (stems) are compared with the available experimental data (dashed lines), demonstrating an excellent agreement, within 1–4 kHz, for the hyperfine splittings. For example, the root-mean square (rms) deviation of the predicted hyperfine splittings from experiment is 2.1 kHz

TABLE I. Strongest predicted *ortho-para* transitions in $H_2^{16}O$ at $T = 296$ K with the $10^{-31}$ cm/molecule intensity cut-off.

| $\nu_1'$ | $\nu_2'$ | $\nu_3'$ | $F'$ | $J'$ | $k_a'$ | $k_c'$ | $I'$ | $E'$ (cm$^{-1}$) | $\nu_1$ | $\nu_2$ | $\nu_3$ | $F$ | $J$ | $k_a$ | $k_c$ | $I$ | $E$ (cm$^{-1}$) | Freq. (cm$^{-1}$) | Int. (cm/molec.) |
|---|---|---|---|---|---|---|---|---|---|---|---|---|---|---|---|---|---|---|---|
| 0 | 1 | 0 | 3 | 4 | 2 | 3 | *o* | 1908.016319 | 0 | 0 | 0 | 4 | 4 | 4 | 0 | *p* | 488.134170 | 1419.882149 | $2.26 \times 10^{-31}$ |
| 0 | 1 | 0 | 3 | 3 | 3 | 1 | *p* | 1907.450231 | 0 | 0 | 0 | 3 | 4 | 3 | 2 | *o* | 382.516901 | 1524.933330 | $1.36 \times 10^{-31}$ |
| 0 | 1 | 0 | 3 | 3 | 3 | 1 | *p* | 1907.450231 | 0 | 0 | 0 | 3 | 4 | 1 | 4 | *o* | 224.838381 | 1682.611850 | $1.12 \times 10^{-31}$ |
| 0 | 1 | 0 | 3 | 4 | 2 | 3 | *o* | 1908.016319 | 0 | 0 | 0 | 3 | 3 | 2 | 2 | *p* | 206.301430 | 1701.714889 | $1.02 \times 10^{-31}$ |
| 0 | 1 | 0 | 3 | 3 | 3 | 1 | *p* | 1907.450231 | 0 | 0 | 0 | 2 | 3 | 1 | 2 | *o* | 173.365811 | 1734.084420 | $2.05 \times 10^{-31}$ |
| 0 | 1 | 0 | 3 | 4 | 2 | 3 | *o* | 1908.016319 | 0 | 0 | 0 | 2 | 2 | 2 | 0 | *p* | 136.163927 | 1771.852392 | $3.28 \times 10^{-31}$ |
| 2 | 1 | 0 | 3 | 4 | 1 | 4 | *o* | 8979.657423 | 0 | 0 | 0 | 4 | 4 | 1 | 3 | *p* | 275.497051 | 8704.160372 | $3.36 \times 10^{-31}$ |
| 2 | 1 | 0 | 3 | 4 | 1 | 4 | *o* | 8979.657423 | 0 | 0 | 0 | 3 | 3 | 1 | 3 | *p* | 142.278493 | 8837.378930 | $1.01 \times 10^{-31}$ |
| 2 | 1 | 0 | 3 | 4 | 1 | 4 | *o* | 8979.657423 | 0 | 0 | 0 | 2 | 2 | 1 | 1 | *p* | 95.175936 | 8884.481487 | $6.41 \times 10^{-31}$ |
| 1 | 1 | 1 | 15 | 14 | 3 | 11 | *o* | 11067.083574 | 0 | 0 | 0 | 14 | 14 | 0 | 14 | *p* | 2073.514207 | 8993.569367 | $1.92 \times 10^{-31}$ |
| 1 | 1 | 1 | 15 | 15 | 2 | 13 | *p* | 11067.089122 | 0 | 0 | 0 | 14 | 13 | 1 | 12 | *o* | 2042.309821 | 9024.779300 | $2.04 \times 10^{-31}$ |

in Fig. 2 a, while for the absolute line positions it is 12.3 kHz. The latter can be explained by the discrepancies in predictions of the pure rotational transitions. The errors in predictions of the hyperfine splittings can be attributed to the level of electronic structure theory, in particular the basis set, employed in the calculations of spin-rotation tensor surface. The basis set convergence of the equilibrium spin-rotation constants of $H_2O$ was investigated elsewhere.[52] According to the results, the employed aug-cc-pwCVTZ basis set produces an average error of 1.3 kHz with a maximum of 1.8 kHz for one of the off-diagonal elements, when compared with the results obtained with the aug-cc-pwCV6Z basis set. There are several predicted splittings in Fig. 2 d–h that are less than 12 kHz and were not resolved in the experiment.[52] Indeed, by visual inspection of the Lamb-dip spectrum plotted in Fig. 1 of ref. 52, which was provided as an example of the experimental resolution achieved in that work, the transition profiles' full width at a half maximum is about 13 kHz.

The sensitivity and resolution required to observe the *ortho-para* transitions in a prospective experiment can be estimated from the simulated absorption spectrum, shown Fig. 3 for selected wavenumber ranges with strong *ortho-para* transitions. Since the Doppler linewidth would be around 0.01 cm$^{-1}$ at room temperature and even much higher-resolution spectroscopy was demonstrated,[69] we used simple Gaussian line profiles with half-width at half-maximum (HWHM) fixed at 0.01, 0.005, and 0.001 cm$^{-1}$ and computed absorption cross sections at $T = 296$ K using `ExoCross`[70] to predict the experimental spectra. The *ortho-para* transitions In Fig. 3 a,c (red) show considerable overlap with the allowed transitions (blue) for purely rotational transitions and in the fundamental $\nu_2$ excitation band and could only be detected with an experimental HWHM below 0.005 cm$^{-1}$ at an experimental sensitivity of $10^{-30}$ and $10^{-29}$ cm$^2$/molecule, respectively. In Fig. 3 b,d, showing parts of the $\nu_2$ and $\nu_2 + \nu_3$ bands, the predicted *ortho-para* transitions are better separated from the allowed transitions and should already be detectable at lower resolution, i. e., at HWHM of 0.01 cm$^{-1}$, but demand a greater sensitivity of $10^{-30}$ and $10^{-31}$ cm$^2$/molecule, respectively. Such high-sensitivity measurements of intensities on the scale of $10^{-30}$ cm$^2$/molecule are currently within reach, for example, using continuous wave laser cavity ring down spectroscopy.[58,71]

## IV. CONCLUSIONS

We developed and performed comprehensive variational calculations of the room temperature linelist of $H_2O$ with hyperfine resolution, including forbidden *ortho-para* transitions. The calculations were based on accurate rovibrational energy levels and wavefunctions produced using the variational approach TROVE. The nuclear hyperfine effects were modeled as spin-rotation and direct spin-spin interactions, with the spin-rotation coupling surface calculated at a high level of the electronic-structure theory. We found excellent agreement between the calculated transition frequencies and available hyperfine-resolved spectroscopic data of allowed transitions.

The predicted *ortho-para* transitions are useful for guiding future experimental spectroscopic studies in search of these forbidden transitions in the laboratory as well as in astrophysical environments. Our accurate predictions of hyperfine effects complement the spectroscopic data for water.

The variational approach we developed for computing these hyperfine effects is general. It includes nuclear quadrupole,[33,34] spin-rotation, and spin-spin interactions, and can be applied to other molecular systems without restrictions on the number and values of nuclear spins.

## SUPPLEMENTARY MATERIAL

The computed hyperfine-linelist data for $H_2O$ are available at `https://doi.org/10.5281/zenodo.6337130`.

Accepted to J. Chem. Phys. 10.1063/5.0090771



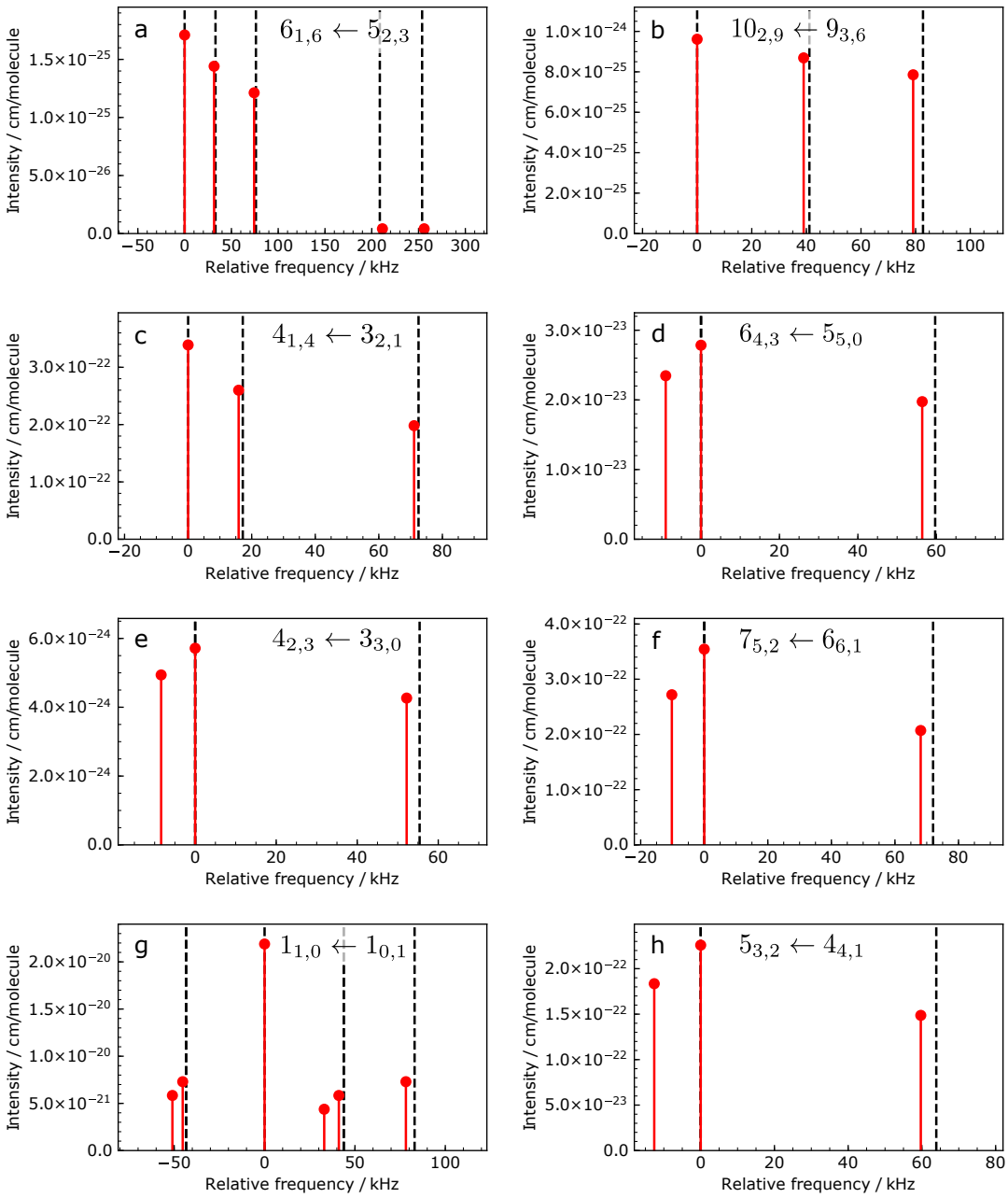


FIG. 2. Comparison of calculated hyperfine transitions (red stems) with experimental data (dashed lines) from (a) ref. 63 and (b-h) ref. 52. Different panels show hyperfine transitions for different rotational bands $J'_{k'_a,k'_c} \leftarrow J_{k_a,k_c}$. The measured (calculated) zero-crossing frequencies, in MHz, are 22235.0447 (22235.0322), 321225.6363 (321225.6311), 380197.3303 (380197.3361), 439150.7746 (439150.7857), 443018.3358 (443018.4016), 448001.0538 (448001.0359), 556935.9776 (556935.9849), 620700.9334 (620700.8889) for panels (a)–(h), respectively.

## AUTHOR DECLARATIONS

### Conflict of interests

The authors have no conflicts to disclose.

## DATA AVAILABILITY

The computer codes used in this work are available from git repositories at `https://github.com/Trovemaster/TROVE` and `https://github.com/CFEL-CMI/richmol`.

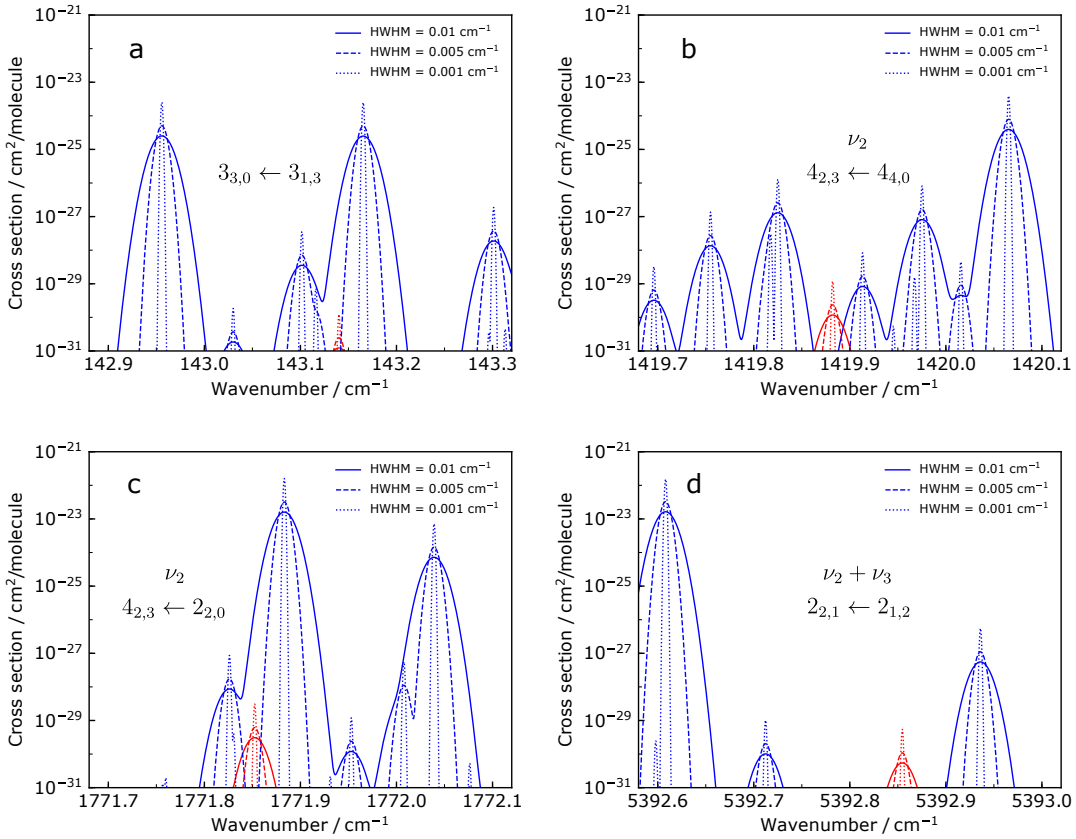


FIG. 3. Absorption cross sections computed at $T = 296$ K for selected rotational bands in (a) ground vibrational state, (b, c) $\nu_2$ and (d) $\nu_2 + \nu_3$ vibrational bands, using Gaussian lineshapes with HWHMs of 0.01 cm$^{-1}$ (solid lines), 0.005 cm$^{-1}$ (dashed lines), and 0.001 cm$^{-1}$ (dotted lines). The cross sections for allowed *ortho-ortho* and *para-para* transitions are plotted with blue colour lines and cross sections for forbidden *ortho-para* transitions are plotted with red colour lines.

## ACKNOWLEDGMENTS

We acknowledge support by Deutsches Elektronen-Synchrotron DESY, a member of the Helmholtz Association (HGF). This work was supported by the Deutsche Forschungsgemeinschaft (DFG) through the priority program "Quantum Dynamics in Tailored Intense Fields" (QUTIF, SPP1840, YA 610/1) and the cluster of excellence "Advanced Imaging of Matter" (AIM, EXC 2056, ID 390715994) and through the Maxwell computational resources operated at Deutsches Elektronen-Synchrotron DESY, Hamburg, Germany. S.Y. acknowledges support from the UK Science and Technology Research Council (STFC, No. ST/R000476/1) and the European Research Council under the European Union's Horizon 2020 research and innovation programme through an Advanced Grant (883830). The authors acknowledge the use of the Cambridge Service for Data Driven Discovery (CSD3), part of which is operated by the University of Cambridge Research Computing on behalf of the STFC DiRAC HPC Facility (www.dirac.ac.uk). The DiRAC component of CSD3 was funded by BEIS capital funding via STFC capital grants ST/P002307/1 and ST/R002452/1 and STFC operations grant ST/R00689X/1. DiRAC is part of the National e-Infrastructure. G.Y. gratefully acknowledges the financial support by the China Scholarship Council (CSC).

[1] P. Cacciani, J. Cosléou, and M. Khelkhal, "Nuclear spin conversion in $H_2O$," Phys. Rev. A **85**, 012521 (2012).
[2] A. Miani and J. Tennyson, "Can ortho–para transitions for water be observed?" J. Chem. Phys. **120**, 2732–2739 (2004).
[3] D. A. Horke, Y.-P. Chang, K. Długołęcki, and J. Küpper, "Separating para and ortho water," Angew. Chem. Int. Ed. **53**, 11965–11968 (2014), arXiv:1407.2056 [physics].
[4] T. Kravchuk, M. Reznikov, P. Tichonov, N. Avidor, Y. Meir, A. Bekkerman, and G. Alexandrowicz, "A magnetically focused molecular beam of ortho-water," Science **331**, 319–321 (2011).
[5] A. Kilaj, H. Gao, D. Rösch, U. Rivero, J. Küpper, and S. Willitsch, "Observation of different reactivities of para- and ortho-water towards trapped diazenylium ions," Nat. Commun. **9**, 2096 (2018).
[6] C. Beduz, M. Carravetta, J. Y.-C. Chen, M. Concistre, M. Denning, M. Frunzi, A. J. Horsewill, O. G. Johannessen, R. Lawler, X. Lei, M. H. Levitt, Y. Li, S. Mamone, Y. Murata, U. Nagel, T. Nishida, J. Ollivier, S. Rols, T. Room, R. Sarkar, N. J. Turro, and Y. Yang, "Quantum rotation of ortho and para-water encapsulated in a fullerene cage," PNAS **109**, 12894–12898 (2012).
[7] M. J. Mumma, H. A. Weaver, and H. P. Larson, "The ortho-para ratio of water vapor in comet P/Halley," Astron. Astrophys. **187**, 419–424 (1987).

[8] E. F. van Dishoeck, E. A. Bergin, D. C. Lis, and J. I. Lunine, "Water: From Clouds to Planets," in *Protostars and Planets VI*, edited by H. Beuther, R. S. Klessen, C. P. Dullemond, and T. Henning (University of Arizona Press, Tucson, 2014) pp. 835–858.

[9] K. Willacy, C. Alexander, M. Ali-Dib, C. Ceccarelli, S. B. Charnley, M. Doronin, Y. Ellinger, P. Gast, E. Gibb, S. N. Milam, O. Mousis, F. Pauzat, C. Tornow, E. S. Wirström, and E. Zicler, "The composition of the protosolar disk and the formation conditions for comets," Space Science Reviews **197**, 151–190 (2015).

[10] H. Kawakita, N. D. Russo, R. Furusho, T. Fuse, J. Watanabe, D. C. Boice, K. Sadakane, N. Arimoto, M. Ohkubo, and T. Ohnishi, "Ortho-to-para ratios of water and ammonia in comet C/2001 Q4 (NEAT): Comparison of nuclear spin temperatures of water, ammonia, and methane," Astrophys. J. **643**, 1337–1344 (2006).

[11] T. Putaud, X. Michaut, F. L. Petit, E. Roueff, and D. C. Lis, "The water line emission and ortho-to-para ratio in the Orion Bar photon-dominated region," Astron. Astrophys. **632**, A8 (2019).

[12] M. R. Hogerheijde, E. A. Bergin, C. Brinch, L. I. Cleeves, J. K. J. Fogel, G. A. Blake, C. Dominik, D. C. Lis, G. Melnick, D. Neufeld, O. Panić, J. C. Pearson, L. Kristensen, U. A. Yıldız, and E. F. van Dishoeck, "Detection of the water reservoir in a forming planetary system," Science **334**, 338–340 (2011).

[13] D. C. Lis, E. A. Bergin, P. Schilke, and E. F. van Dishoeck, "*Ortho*-to-*Para* ratio in interstellar water on the sightline toward sagittarius B2(N)," J. Phys. Chem. A **117**, 9661–9665 (2013).

[14] N. Flagey, P. F. Goldsmith, D. C. Lis, M. Gerin, D. Neufeld, P. Sonnentrucker, M. D. Luca, B. Godard, J. R. Goicoechea, R. Monje, and T. G. Phillips, "Water absorption in galactic translucent clouds: Conditions and history of the gas derived from *Herschel*/HIFI PRISMAS observations," Astrophys. J. **762**, 11 (2012).

[15] E. F. van Dishoeck, E. Herbst, and D. A. Neufeld, "Interstellar water chemistry: From laboratory to observations," Chem. Rev. **113**, 9043–9085 (2013).

[16] R. F. Curl Jr, J. V. V. Kasper, and K. S. Pitzer, "Nuclear spin state equilibration through nonmagnetic collisions," J. Chem. Phys. **46**, 3220 (1967).

[17] P. L. Chapovsky and L. J. F. Hermans, "Nuclear spin conversion in polyatomic molecules," Annu. Rev. Phys. Chem. **50**, 315–345 (1999).

[18] Z.-D. Sun, K. Takagi, and F. Matsushima, "Separation and conversion dynamics of four nuclear spin isomers of ethylene," Science **310**, 1938–1941 (2005).

[19] E. Ilisca, "Ortho-para conversion of hydrogen molecules physisorbed on surfaces," Prog. Surf. Sci. **41**, 217–335 (1992).

[20] P. L. Chapovsky, "Hyperfine spectra of $CH_3F$ nuclear spin conversion," J. Phys. B **33**, 1001–1011 (2000).

[21] P. L. Chapovsky, "Conversion of nuclear spin isomers of water molecules under ultracold conditions of space," Quantum Electron. **49**, 473–478 (2019).

[22] D. Hollenbach, M. J. Kaufman, E. A. Bergin, and G. J. Melnick, "Water, $O_2$, and ice in molecular clouds," Astrophys. J. **690**, 1497–1521 (2008).

[23] T. Hama, N. Watanabe, A. Kouchi, and M. Yokoyama, "Spin temperature of water molecules desorbed from the surfaces of amorphous solid water, vapor-deposited and produced from photolysis of a $CH_4/O_2$ solid mixture," Astrophys. J. **738**, L15 (2011).

[24] T. Hama, A. Kouchi, and N. Watanabe, "Statistical ortho-to-para ratio of water desorbed from ice at 10 kelvin," Science **351**, 65–67 (2015).

[25] T. Hama, A. Kouchi, and N. Watanabe, "The ortho-to-para ratio of water molecules desorbed from ice made from para-water monomers at 11 K," Astrophys. J. Lett. **857**, L13 (2018).

[26] R. Sliter, M. Gish, and A. F. Vilesov, "Fast nuclear spin conversion in water clusters and ices: A matrix isolation study," J. Phys. Chem. A **115**, 9682–9688 (2011).

[27] Y. Liu and L. Luo, "Molecular collisions: From near-cold to ultra-cold," Front. Phys. **16**, 42300 (2021).

[28] S. N. Yurchenko, W. Thiel, and P. Jensen, "Theoretical ROVibrational Energies (TROVE): A robust numerical approach to the calculation of rovibrational energies for polyatomic molecules," J. Mol. Spectrosc. **245**, 126–140 (2007).

[29] A. Yachmenev and S. N. Yurchenko, "Automatic differentiation method for numerical construction of the rotational-vibrational Hamiltonian as a power series in the curvilinear internal coordinates using the Eckart frame," J. Chem. Phys. **143**, 014105 (2015).

[30] S. N. Yurchenko, A. Yachmenev, and R. I. Ovsyannikov, "Symmetry adapted ro-vibrational basis functions for variational nuclear motion calculations: TROVE approach," J. Chem. Theory Comput. **13**, 4368 (2017), arXiv:1708.07185 [physics].

[31] K. L. Chubb, A. Yachmenev, J. Tennyson, and S. N. Yurchenko, "Treating linear molecule HCCH in calculations of rotation-vibration spectra," J. Chem. Phys. **149**, 014101 (2018).

[32] I. I. Mizus, A. A. Kyuberis, N. F. Zobov, V. Y. Makhnev, O. L. Polyansky, and J. Tennyson, "High-accuracy water potential energy surface for the calculation of infrared spectra," Philosophical Transactions of the Royal Society A: Mathematical, Physical and Engineering Sciences **376**, 20170149 (2018).

[33] A. Yachmenev and J. Küpper, "Communication: General variational approach to nuclear-quadrupole coupling in rovibrational spectra of polyatomic molecules," J. Chem. Phys. **147**, 141101 (2017), arXiv:1709.08558 [physics].

[34] A. Yachmenev, L. V. Thesing, and J. Küpper, "Laser-induced dynamics of molecules with strong nuclear quadrupole coupling," J. Chem. Phys. **151**, 244118 (2019), arXiv:1910.13275 [physics].

[35] W. H. Flygare, "Magnetic interactions in molecules and an analysis of molecular electronic charge distribution from magnetic parameters," Chem. Rev. **74**, 653–687 (1974).

[36] R. N. Zare, *Angular Momentum* (John Wiley & Sons, New York, NY, USA, 1988).

[37] A. Owens and A. Yachmenev, "RichMol: A general variational approach for rovibrational molecular dynamics in external electric fields," J. Chem. Phys. **148**, 124102 (2018), arXiv:1802.07603 [physics].

[38] C. Saribal, G. Yang, E. Zak, Y. Saleh, J. Eggers, V. Sanjay, A. Yachmenev, and J. Küpper, "Richmol: Python package for variational simulations of molecular nuclear motion dynamics in fields," Comp. Phys. Comm. , in preparation (2021), the current version of the software is available at `https://github.com/CFEL-CMI/richmol`.

[39] J. K. G. Watson, "Aspects of quartic and sextic centrifugal effects on rotational energy levels," in *Vibrational Spectra and Structure*, Vol. 6, edited by J. R. Durig (Marcel Dekker, 1977) p. 1.

[40] K. A. Peterson and T. H. Dunning, "Accurate correlation consistent basis sets for molecular core–valence correlation effects: The second row atoms Al–Ar, and the first row atoms B–Ne revisited," J. Chem. Phys. **117**, 10548–10560 (2002).

[41] T. H. Dunning, "Gaussian basis sets for use in correlated molecular calculations. I. The atoms boron through neon and hydrogen," J. Chem. Phys. **90**, 1007 (1989).

[42] R. A. Kendall, T. H. Dunning, Jr., and R. J. Harrison, "Electron affinities of the first-row atoms revisited. Systematic basis sets and wave functions," J. Chem. Phys. **96**, 6796–6806 (1992).

[43] B. P. Pritchard, D. Altarawy, B. Didier, T. D. Gibson, and T. L. Windus, "New basis set exchange: An open, up-to-date resource for the molecular sciences community," J. Chem. Inf. Model. **59**, 4814–4820 (2019).

[44] D. Feller, "The role of databases in support of computational chemistry calculations," J. Comput. Chem. **17**, 1571–1586 (1996).

[45] K. L. Schuchardt, B. T. Didier, T. Elsethagen, L. Sun, V. Gurumoorthi, J. Chase, J. Li, and T. L. Windus, "Basis set exchange: A community database for computational sciences," J. Chem. Inf. Model. **47**, 1045–1052 (2007).

[46] G. E. Scuseria, "Analytic evaluation of energy gradients for the singles and doubles coupled cluster method including perturbative triple excitations: Theory and applications to FOOF and $Cr_2$," J. Chem. Phys. **94**, 442–447 (1991).

[47] J. Gauss, K. Ruud, and T. Helgaker, "Perturbation-dependent atomic orbitals for the calculation of spin-rotation constants and rotational $g$ tensors," J. Chem. Phys. **105**, 2804–2812 (1996).

[48] J. Gauss and D. Sundholm, "Coupled-cluster calculations of spin-rotation constants," Mol. Phys. **91**, 449–458 (1997).

[49] J. F. Stanton, J. Gauss, L. Cheng, M. E. Harding, D. A. Matthews, and P. G. Szalay, "CFOUR, Coupled-Cluster techniques for Computational Chemistry, a quantum-chemical program package," With contributions from A.A. Auer, R.J. Bartlett, U. Benedikt, C. Berger, D.E. Bernholdt, S. Blaschke, Y. J. Bomble, S. Burger, O. Christiansen, D. Datta, F. Engel, R. Faber, J. Greiner, M. Heckert, O. Heun, M. Hilgenberg, C. Huber, T.-C. Jagau, D. Jonsson, J. Jusélius, T. Kirsch, K. Klein, G.M. KopperW.J. Lauderdale, F. Lipparini, T. Metzroth, L.A. Mück, D.P. O'Neill, T. Nottoli, D.R. Price, E. Prochnow, C. Puzzarini, K. Ruud, F. Schiffmann, W. Schwalbach, C. Simmons, S. Stopkowicz, A. Tajti, J. Vázquez, F. Wang, J.D. Watts and the integral packages MOLECULE (J. Almlöf and P.R. Taylor), PROPS (P.R. Taylor), ABACUS (T. Helgaker, H.J. Aa. Jensen, P. Jørgensen, and J. Olsen), and ECP routines by A. V. Mitin and C. van Wüllen. For the current version, see http://www.cfour.de.

[50] S. N. Yurchenko and T. M. Mellor, "Treating linear molecules in calculations of rotation-vibration spectra," J. Chem. Phys. **153**, 154106 (2020).

[51] A. Yachmenev, S. N. Yurchenko, I. Paidarová, P. Jensen, W. Thiel, and S. P. A. Sauer, "Thermal averaging of the indirect nuclear spin-spin coupling constants of ammonia: The importance of the large amplitude inversion mode," J. Chem. Phys. **132**, 114305 (2010).

[52] G. Cazzoli, C. Puzzarini, M. E. Harding, and J. Gauss, "The hyperfine structure in the rotational spectrum of water: Lamb-dip technique and quantum-chemical calculations," Chem. Phys. Lett. **473**, 21–25 (2009).

[53] B. V. Noumerov, "A method of extrapolation of perturbations," Mon. Not. R. Astron. Soc. **84**, 592–602 (1924).

[54] J. W. Cooley, "An improved eigenvalue corrector formula for solving the Schrödinger equation for central fields," Math. Comput. **15**, 363–374 (1961).

[55] J. Tennyson, P. F. Bernath, L. R. Brown, A. Campargue, A. G. Császár, L. Daumont, R. R. Gamache, J. T. Hodges, O. V. Naumenko, O. L. Polyansky, L. S. Rothman, A. C. Vandaele, N. F. Zobov, A. R. A. Derzi, C. Fábri, A. Z. Fazliev, T. Furtenbacher, I. E. Gordon, L. Lodi, and I. I. Mizus, "IUPAC critical evaluation of the rotational–vibrational spectra of water vapor, part III: Energy levels and transition wavenumbers for $H_2{}^{16}O$," J. Quant. Spectrosc. Radiat. Transf. **117**, 29–58 (2013).

[56] J. Tennyson, S. N. Yurchenko, A. F. Al-Refaie, V. H. Clark, K. L. Chubb, E. K. Conway, A. Dewan, M. N. Gorman, C. Hill, A. Lynas-Gray, T. Mellor, L. K. McKemmish, A. Owens, O. L. Polyansky, M. Semenov, W. Somogyi, G. Tinetti, A. Upadhyay, I. Waldmann, Y. Wang, S. Wright, and O. P. Yurchenko, "The 2020 release of the ExoMol database: Molecular line lists for exoplanet and other hot atmospheres," J. Quant. Spectrosc. Radiat. Transf. **255**, 107228 (2020).

[57] A. Campargue, A. M. Solodov, A. A. Solodov, A. Yachmenev, and S. N. Yurchenko, "Detection of electric-quadrupole transitions in water vapour near 5.4 and 2.5 $\mu$m," Phys. Chem. Chem. Phys. **22**, 12476–12481 (2020).

[58] A. Campargue, S. Kassi, A. Yachmenev, A. A. Kyuberis, J. Küpper, and S. N. Yurchenko, "Observation of electric-quadrupole infrared transitions in water vapor," Phys. Rev. Research **2**, 023091 (2020), arXiv:2001.02922 [physics].

[59] H. Fleurbaey, R. Grilli, D. Mondelain, S. Kassi, A. Yachmenev, S. N. Yurchenko, and A. Campargue, "Electric-quadrupole and magnetic-dipole contributions to the $\nu_2 + \nu_3$ band of carbon dioxide near 3.3 $\mu$m," J. Quant. Spectrosc. Radiat. Transf. **266**, 107558 (2021).

[60] A. Yachmenev, A. Campargue, S. N. Yurchenko, J. Küpper, and J. Tennyson, "Electric quadrupole transitions in carbon dioxide," J. Chem. Phys. **154**, 211104 (2021).

[61] O. L. Polyansky, A. A. Kyuberis, N. F. Zobov, J. Tennyson, S. N. Yurchenko, and L. Lodi, "ExoMol molecular line lists XXX: a complete high-accuracy line list for water," Mon. Not. R. Astron. Soc. **480**, 2597–2608 (2018).

[62] J. Tennyson, S. N. Yurchenko, A. F. Al-Refaie, E. J. Barton, K. L. Chubb, P. A. Coles, S. Diamantopoulou, M. N. Gorman, C. Hill, A. Z. Lam, L. Lodi, L. K. McKemmish, Y. Na, A. Owens, O. L. Polyansky, T. Rivlin, C. Sousa-Silva, D. S. Underwood, A. Yachmenev, and E. Zak, "The ExoMol database: Molecular line lists for exoplanet and other hot atmospheres," J. Mol. Spectrosc. **327**, 73–94 (2016), new Visions of Spectroscopic Databases, Volume {II}.

[63] H. Bluyssen, A. Dymanus, and J. Verhoeven, "Hyperfine structure of $H_2O$ and HDSe by beam-maser spectroscopy," Phys. Lett. A **24**, 482–483 (1967).

[64] S. Kassi and A. Campargue, "Cavity ring down spectroscopy with $5 \times 10^{-13}$ cm$^{-1}$ sensitivity," J. Chem. Phys. **137**, 234201 (2012).

[65] E. Karlovets, S. Kassi, and A. Campargue, "High sensitivity CRDS of $CO_2$ in the 1.18 $\mu$m transparency window. Validation tests of current spectroscopic databases," J. Quant. Spectrosc. Radiat. Transfer **247**, 106942 (2020).

[66] R. Tóbiás, T. Furtenbacher, I. Simkó, A. G. Császár, M. L. Diouf, F. M. J. Cozijn, J. M. A. Staa, E. J. Salumbides, and W. Ubachs, "Spectroscopic-network-assisted precision spectroscopy and its application to water," Nat. Commun. **11**, 1708 (2020).

[67] S. G. Kukolich, "Measurement of the molecular $g$ values in $H_2O$ and $D_2O$ and hyperfine structure in $H_2O$," J. Chem. Phys. **50**, 3751–3755 (1969).

[68] G. Golubiatnikov, V. Markov, A. Guarnieri, and R. Knöchel, "Hyperfine structure of $H_2{}^{16}O$ and $H_2{}^{18}O$ measured by Lamb-dip technique in the 180–560 GHz frequency range," J. Mol. Spectrosc. **240**, 251–254 (2006).

[69] C. Daussy, T. Marrel, A. Amy-Klein, C. T. Nguyen, C. J. Bordé, and C. Chardonnet, "Limit on the parity nonconserving energy difference between the enantiomers of a chiral molecule by laser spectroscopy," Phys. Rev. Lett. **83**, 1554–1557 (1999).

[70] S. N. Yurchenko, A. F. Al-Refaie, and J. Tennyson, "ExoCross: a general program for generating spectra from molecular line lists," Astron. Astrophys. **614**, A131 (2018), arXiv:1801.09803 [astro-ph.EP].

[71] A. Campargue, S. Kassi, K. Pachucki, and J. Komasa, "The absorption spectrum of $H_2$: CRDS measurements of the (2-0) band, review of the literature data and accurate *ab initio* line list up to 35 000 cm$^{-1}$," Phys. Chem. Chem. Phys. **14**, 802–815 (2011).

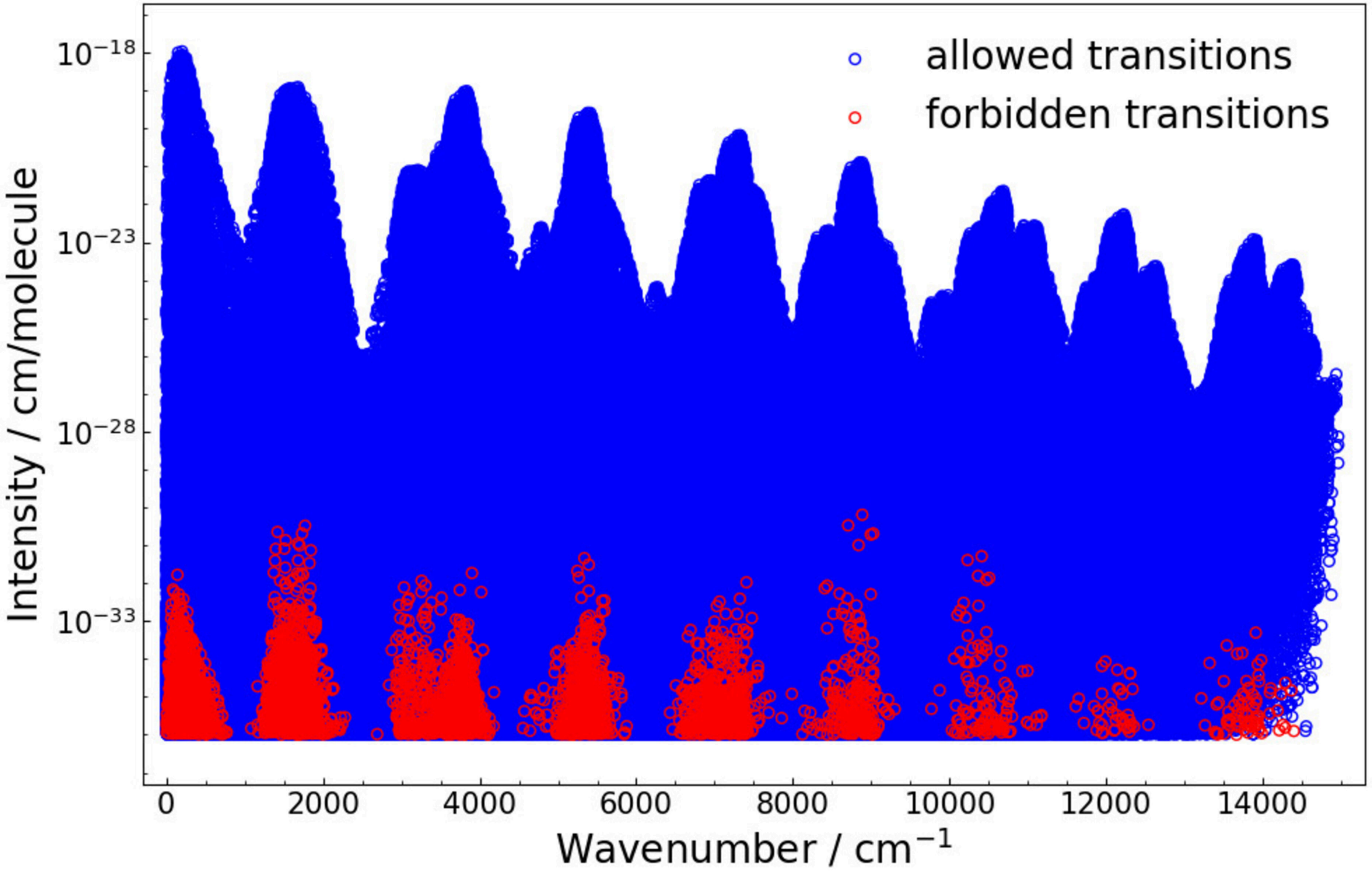
allowed transitions
forbidden transitions
$10^{-18}$
$10^{-23}$
$10^{-28}$
$10^{-33}$
Intensity / cm/molecule
0
2000
4000
6000
8000
10000
12000
14000
Wavenumber / $cm^{-1}$

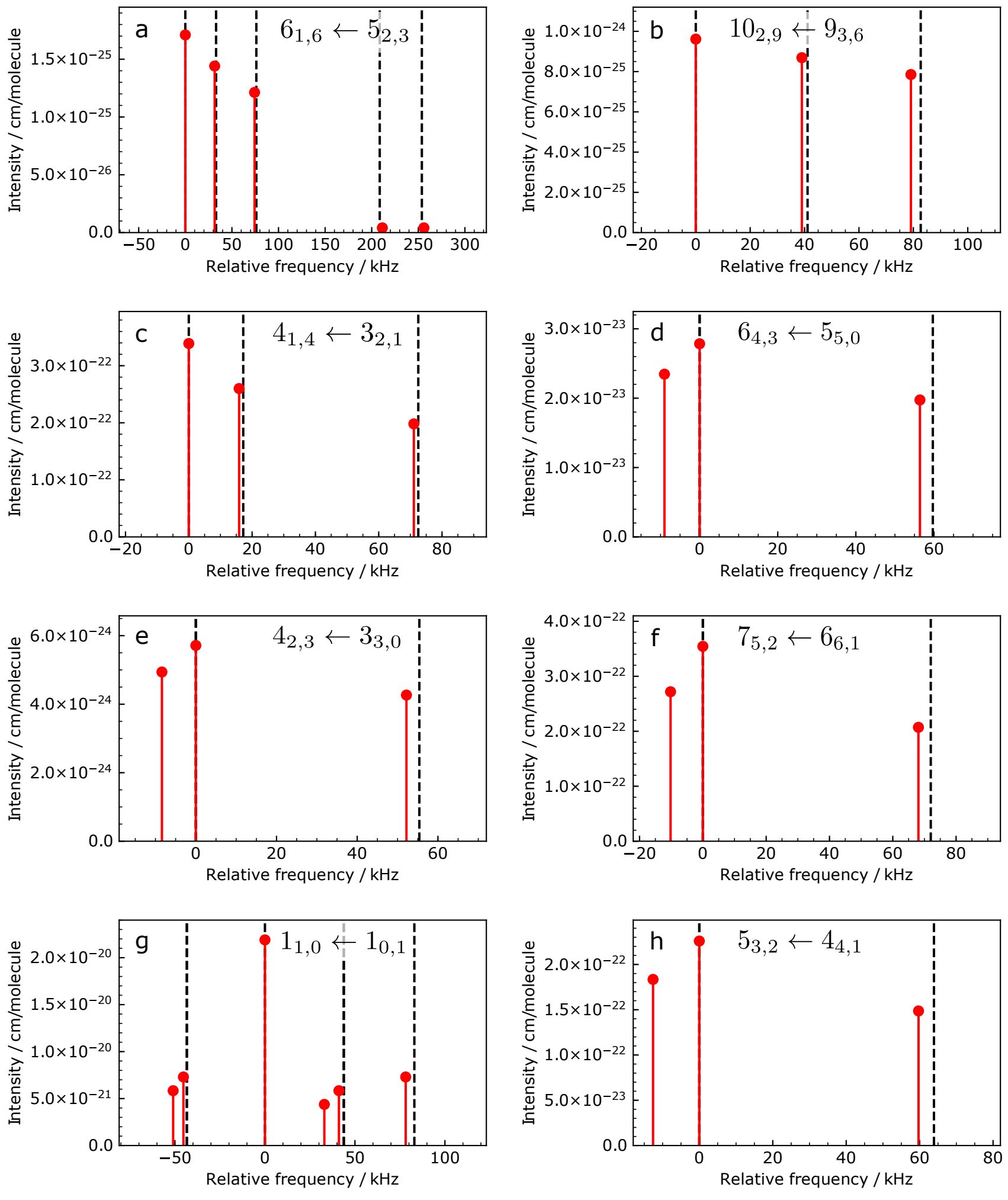
a
$6_{1,6} \leftarrow 5_{2,3}$
b
$10_{2,9} \leftarrow 9_{3,6}$
c
$4_{1,4} \leftarrow 3_{2,1}$
d
$6_{4,3} \leftarrow 5_{5,0}$
e
$4_{2,3} \leftarrow 3_{3,0}$
f
$7_{5,2} \leftarrow 6_{6,1}$
g
$1_{1,0} \leftarrow 1_{0,1}$
h
$5_{3,2} \leftarrow 4_{4,1}$
Intensity / cm/molecule
Relative frequency / kHz

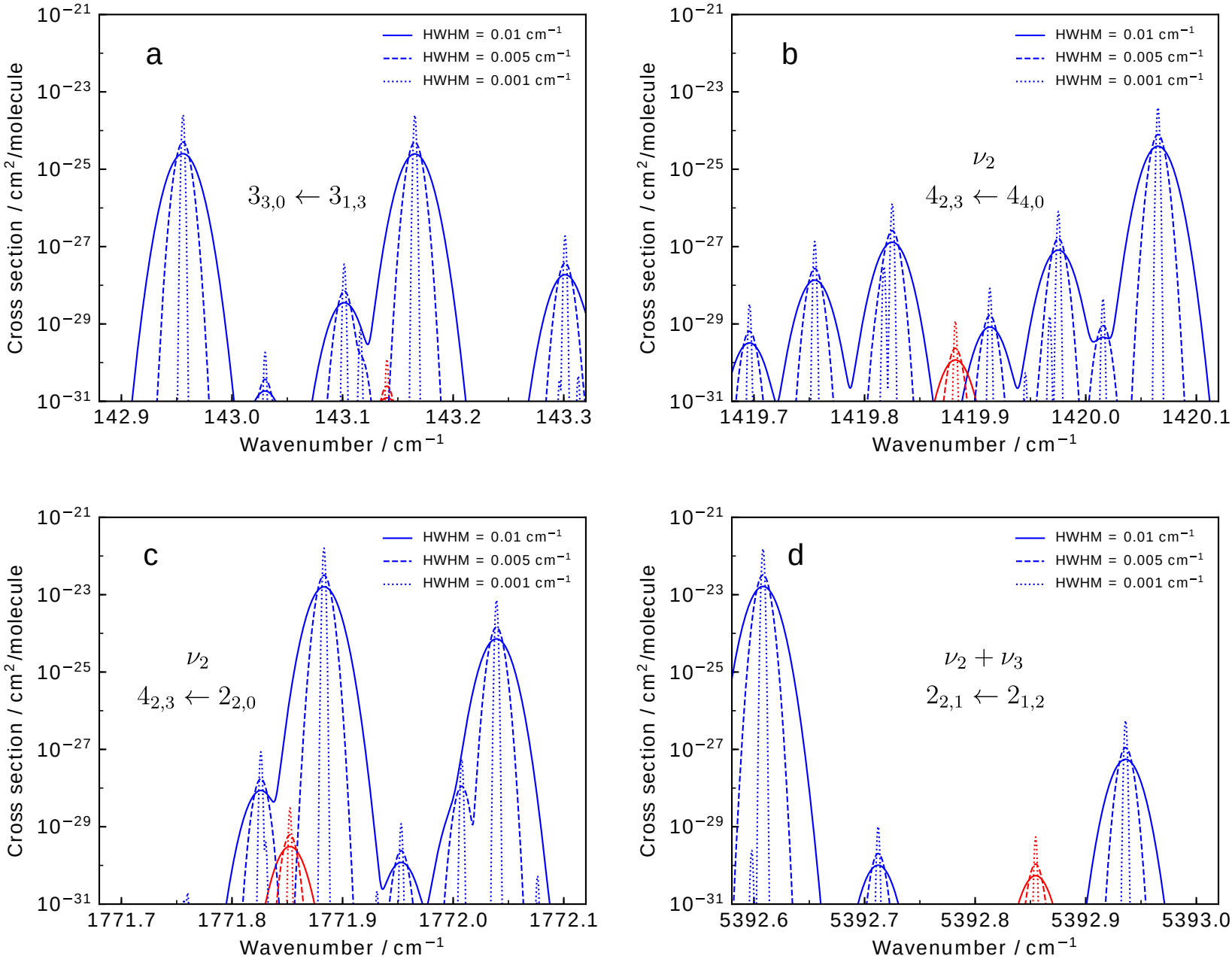
a
HWHM = 0.01 cm$^{-1}$
HWHM = 0.005 cm$^{-1}$
HWHM = 0.001 cm$^{-1}$
$3_{3,0} \leftarrow 3_{1,3}$
Cross section / cm$^2$/molecule
Wavenumber / cm$^{-1}$
b
$\nu_2$
$4_{2,3} \leftarrow 4_{4,0}$
c
$\nu_2$
$4_{2,3} \leftarrow 2_{2,0}$
d
$\nu_2 + \nu_3$
$2_{2,1} \leftarrow 2_{1,2}$